

Unraveling the quenching of star formation: a comparison of the results of a bulge-disk decomposition between Green Valley and Star Forming galaxies

A. C. Santiago-Menezes, A. Schnorr Müller, M. Trevisan, F. Palacios, & C. A. Oliveira

¹ Universidade Federal do Rio Grande do Sul
e-mail: ana.santiago@ufrgs.br

Abstract. Previous studies have shown that the probability of a galaxy having ceased its star formation is primarily linked to morphological parameters such as velocity dispersion and concentration. The origin of this relation isn't clear: it's possible that entry into the Green Valley is associated with an increase in velocity dispersion and concentration. Alternatively, galaxies with higher concentrations and velocity dispersions might be more susceptible to the quenching process. To identify the processes responsible for the cessation of star formation and establish connections between them and morphological changes, we examined a sample of central galaxies from the Green Valley and two control samples of central galaxies from the Main Sequence. One of these control samples was matched solely based on mass and redshift with the Green Valley sample, while the other was matched based on mass, redshift, concentration, and central velocity dispersion. We compared morphological parameters obtained from bulge-disk decompositions and assessed the prevalence of structures such as rings, bars, and classical bulges. To do this, we utilized deep, high-resolution images in the g and r bands obtained with the Subaru Telescope as part of the Hyper Suprime-Cam Subaru Strategic Program. Through morphological comparisons, we observed that the absence of structural differences in the sample matched by morphological parameters suggests that morphology is the primary factor contributing to the potential excess of these structures in the Green Valley.

Resumo. Estudos anteriores mostraram que a probabilidade de uma galáxia ter cessado sua formação estelar está relacionada, principalmente, a parâmetros morfológicos, como dispersão de velocidades e concentração. A origem dessa relação não é clara: é possível que a entrada ao *Green Valley* esteja relacionada com um aumento de dispersão de velocidades e concentração. Alternativamente, galáxias com maiores concentrações e dispersões de velocidade podem ser mais suscetíveis ao processo de *quenching*. Com o objetivo de identificar os processos responsáveis pela cessação da formação estelar e colocar vínculos nos cenários que os relacionam a mudanças morfológicas, estudamos uma amostra de galáxias centrais do *Green Valley* e duas amostras de controle de galáxias centrais da *Main Sequence*, uma delas pareada com a amostra do *Green Valley* somente em massa e *redshift*, e outra pareada em massa, *redshift*, concentração e dispersão de velocidades central. Comparamos parâmetros morfológicos obtidos com decomposições bojo-disco, além de compararmos a prevalência de estruturas como anéis, barras e bojos clássicos. Para isso, fizemos uso de imagens profundas e de alta resolução nas bandas g e r , obtidas com o telescópio Subaru como parte do *Hyper Suprime-Cam Subaru Strategic Program*. Com os comparativos morfológicos, vimos que a ausência de diferenças estruturais na amostra pareada por parâmetros morfológicos, nos aponta que a morfologia é o fator que mais contribui para o excesso, reportado em trabalhos anteriores, dessas estruturas no *Green Valley*.

Keywords. Galaxies: bulge – evolution – photometry

1. Introduction

In a diagram that relates a galaxy's stellar mass to its star formation rate, two density peaks are observed: one associated with galaxies in the Star Forming group, characterized by bluer colors and high rates of star formation; while the other refers to passive galaxies, which are redder and lack evidence of recent star formation. The Green Valley is an intermediate region (Salim, S. 2015) in this diagram and is believed to be a transitional zone between the two major groups as star formation rates decrease.

In this work, we were interested in determining the prevalence of morphological structures such as bars, rings and classical bulges in the Green Valley and Star Forming control samples, as it will allow us to put constraints on scenarios which predict that entrance into the Green Valley is associated to morphological changes.

2. Data

We utilized deep and high-resolution images in the g and r bands obtained with the Subaru Telescope 8.2m as part of the Hyper Suprime-Cam Subaru Strategic Program (HSC) (Aihara, H. et

al. 2022). Other data, such as stellar masses and star formation rates, were obtained from the GALEX-SDSS-WISE LEGACY CATALOG (GSWLC-2) (Salim, S. et al. 2018). Using the classification from Lim, S. et al. (2017), we selected only central galaxies to reduce environmental effects in our samples. We classified galaxies into three groups based on their star formation rate, following the criteria of Trussler, J. et al. (2020). We ended up with three samples, each containing 58 galaxies, with redshifts between $0.02 < z < 0.05$:

- Green Valley galaxies;
- Star Forming galaxies matched in mass and redshift.
- Star Forming galaxies matched in mass, redshift, velocity dispersion and concentration.

This last one is comprised of galaxies with similar morphologies to those in the Green Valley.

3. Methods

For each of the three analyzed samples, we performed bulge-disk decompositions using the Imfit software (Erwin, P. 2015). Our

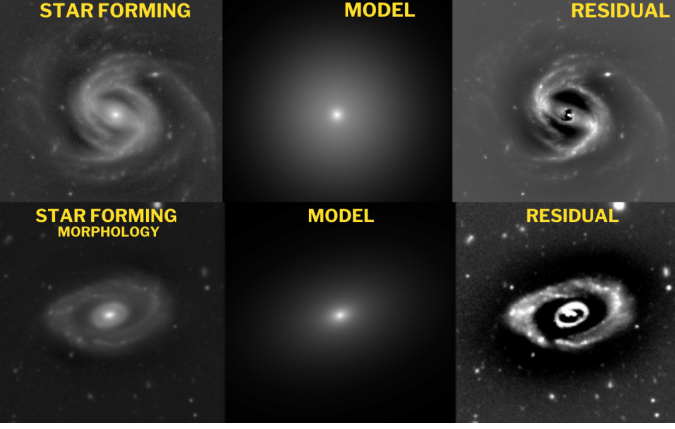


FIGURE 1. Examples of galaxies and their models and residual maps. The upper panel shows a barred spiral galaxy and the bottom panel shows a galaxy with a ring.

Table 1. p-values from Fisher tests comparing Green Valley galaxies (GV), Star Forming galaxies matched only in mass and redshift (SF) and Star Forming galaxies matched in mass, redshift, velocity dispersion and concentration (SFmorph).

Samples	Spiral arms	Bars	Rings
GV e SF	$p\text{-value} = 0.103$	0.504	0.099
GV e SFmorph	$p\text{-value} = 0.643$	0.815	0.824

decompositions were conducted by fitting galaxy images using two-dimensional Sérsic components, one to represent the disk (with a Sérsic index $n = 1$) and another to represent the bulge (with a free n). From the fits performed we obtain the best fitting effective radii, position angle, ellipticity and intensities at effective radii for each component, the Sérsic index of the bulge component and the bulge-to-total luminosity ratio.

Structures such as bars, rings and spiral arms were identified based on a visual inspection of the images and residual maps. To ensure that the light from objects near the target galaxies did not affect the fit, we used masks created by the SourceExtractor software (Bertin, E. e Arnouts, S. 1996).

4. Results

We found no differences between our samples regarding the prevalence of bars or rings, showing how important it is to use high resolution images. This suggests that previous reports of an excess of bars in the Green Valley might be due to the limited resolution of Sloan Digital Sky Survey data making the detection of bars more difficult in low mass galaxies, as suggested by Erwin, P. (2018).

The largest difference between the samples is observed in the Sérsic index of the Bulge; Star Forming galaxies matched in mass and redshift have a significantly larger fraction of galaxies with $n \approx 1$, as seen in the left panel of Fig.3. To investigate the reason for this, we classify the bulges as classical or pseudobulges, with pseudobulges satisfying the criteria $n < 2$ and $B/T < 0.3$. In the right panel of Fig.3 we show the distribution of n for the galaxies hosting pseudobulges. It is apparent that the larger number of galaxies with $n \approx 1$ in the Star Forming sample matched in z and $\log M_\odot$ is due to a larger fraction of pseudobulges. Considering that the origins of classical bulges and pseudobulges are quite different - classical bulges originate in galaxy mergers or violent disk instabilities at high redshifts while pseudobulges are built by secular processes - this result suggest that

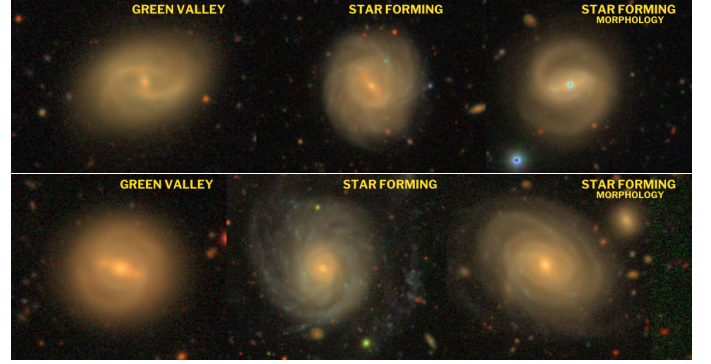


FIGURE 2. HSC images of galaxies with $10 < \log(M/M_\odot) < 10.5$ (upper panel) and $10.5 < \log(M/M_\odot) < 11$ (bottom panel). Star Forming galaxies matched in mass and redshift at the central and Star Forming galaxies matched in mass, redshift, velocity dispersion and concentration on the right.

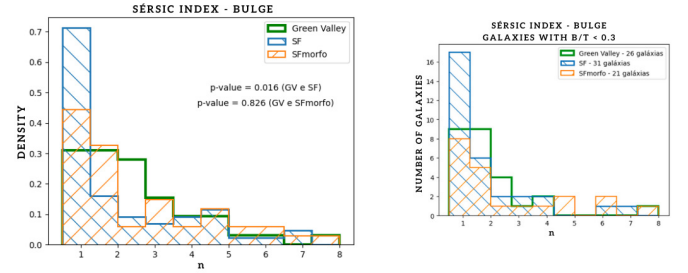


FIGURE 3. Sérsic index distributions for the three samples and their p-values obtained from the KS test (on the left) and Sérsic index distribution for galaxies with $B/T < 0.3$ (on the right).

galaxies that experienced violent processes at high redshift are more likely to enter the Green Valley.

References

- Aihara, H. et al. (2022). Third data release of the hyper supprime-cam Subaru strategic program. Publications of the Astronomical Society of Japan, 74(2):247–272.
- Bertin, E. e Arnouts, S. (1996). SExtractor: Software for source extraction. , 117:393–404
- Erwin, P. (2015). IMFIT: A Fast, Flexible New Program for Astronomical Image Fitting., 799(2):226.
- Erwin, P. (2018). The dependence of bar frequency on galaxy mass, colour, and gas content—and angular resolution—in the local universe. Monthly Notices of the Royal Astronomical Society, 474(4):5372–5392.
- Gao, H., Ho, L. C., Barth, A. J., e Li, Z.-Y. (2018). The carnegie-irvine galaxy survey. vii. constraints on the origin of s0 galaxies from their photometric structure. The Astrophysical Journal, 862(2):100
- Lim, S., Mo, H., Lu, Y., Wang, H., e Yang, X. (2017). Galaxy groups in the low-redshift universe. Monthly Notices of the Royal Astronomical Society, 470(3):2982–3005.
- Salim, S. (2015). Green valley galaxies. arXiv preprint arXiv:1501.01963.
- Salim, Samir, Médéric Boquien, and Janice C. Lee. "Dust attenuation curves in the local universe: demographics and new laws for star-forming galaxies and high-redshift analogs." The Astrophysical Journal 859.1 (2018): 11.
- Trussler, J., Maiolino, R., Maraston, C., Peng, Y., Thomas, D., Goddard, D., e Lian, J. (2020). Both starvation and outflows drive galaxy quenching. Monthly Notices of the Royal Astronomical Society, 491(4):5406–5434.